

This is accepted version of the paper:

"An analysis of optimal segmented flight design in a rotary dryer" by Franck Lominé , Mustapha Hellou and Yves Roques

published in Powder Technology 407 (2022) 117594

See <https://doi.org/10.1016/j.powtec.2022.117594>

An analysis of optimal segmented flight design in a rotary dryer

Franck Lominé ^{a,*} , Mustapha Hellou ^a , Yves Roques ^b

^a University of Rennes, INSA Rennes LGCGM (Laboratoire de Génie Civil et Génie Mécanique) 35708 Rennes, France

^b CMI Roullier, Dinard, France

ARTICLE INFO

Keywords:

Rotary dryer
Powder
Granular material
Drum
Flight design
Dryer performance
Falling time in drum

ABSTRACT

In this paper, an analysis of the optimal design for two-segmented flight is performed with the aim to obtain some practical recommendations for the design of a rotary dryer. Using a geometrical model, validated with experimental results, flight loading and unloading are studied over the range of every possible angle between the flight segments. Maximum volume carried out by the flight, the maximum discharging angle and the mean falling height of material are computed for all configurations. Influence of size ratio between segments and drum radius are also investigated. By determining the curtain filling degree and the cumulative transfer area of material over one drum revolution, we estimate what the best flight design is, in order to maximise the contact surface between material and air flow necessary to increase the dryer performance.

1. Introduction

Rotary dryers are widely used in industrial processes to dry particulate solids [1–3]. This kind of dryer is made of a rotating tube that can be slightly inclined to induce solid flow in the longitudinal direction. Wet granular material is usually injected into the dryer through a hot temperature air stream. Due to the tube rotation, the air stream, the

presence of flights and a possible drum slope, the granular material progressively moves to the drum exit.

The hot stream provides the heat required for vaporisation of the water content in the granular material. To promote contact between the solid and the air stream, the material is usually lifted with flights disposed all around the interior lateral surface of the tube. According to the technological configuration of the system, the flights can also be

* Corresponding author.

E-mail address: franck.lomine@insa-rennes.fr (F. Lominé).

used through a positive or negative slope to modify the transverse movement of the material. On the whole, the movement of solid particles inside the dryer can be decomposed into successive cascading steps [4,5].

Improving rotary dryer design to reduce power consumption and provide a better quality control of the final product, is of major interest to industries dealing with such equipments. For this reason, rotary dryers have been and are still widely studied theoretically [4–8], experimentally [8–11] and numerically [12–14]. Design of dryers is very important to control the drying performance. Nevertheless, giving general recommendations on the design is not an easy step because of the influence of the variety of geometrical and physical parameters, and also of the material properties.

Some studies focus on granular material behaviour inside such drums [15–18]. Others try to analyse and describe thermal effects during such process [12,19–21]. The last are concerned with dryer optimisation based on geometrical considerations and basic material properties such as repose angle. Among this last group of studies, some are more focused on mean residence time (MRT) prediction inside a rotary drum [5,22], while others are more interested in how flight shape influences cascading patterns through falling height and volume of material carried and released by the flights. Our paper belongs to this last category of studies.

Hodgson and Keast [23] performed a series of experiments to determine the unloading rate of flights of an industrial sugar dryer. They measure the time it takes to fill a collection vessel at different locations to determine the unloading profile of the flights. Baker [24] presented a geometrical model to estimate solid holdup within two types of flights (angled flight and extended-circular flight) depending on the dryer, the flight geometry and dynamic angle of repose of the material. Then he calculated, with his model, the maximum number of flights that can be disposed on the circumference of the drum by ensuring flight loading at full capacity.

Kelly [25] calculated the unloading rate of flights and developed a theoretical flight geometry that would ensure uniform distribution of solids across the dryer. This profile is referred as “Equal Angular Distribution” (EAD) profile.

Wang et al. [26] developed a geometrical model for the unloading of a two segment flight and expressed the cross-sectional area of the solid in the flight as a function of the flight angular position, the angular velocity of the drum and the material repose angle. They used this model to determine the discharging rate and the retention time as a function of the operating parameters.

Revol et al. [27] developed correlations to determine the solid holdup in a flight constituted with two or three segments. These correlations were used to calculate the discharging rate of flights. A comparison of their results with experimental data shows relatively good agreement in flight holdup while significant difference between model prediction and experimental results were observed for the discharging rate. According to the authors, the discrepancy between prediction and measurement suggests that the dynamic angle of repose is not independent of the shape of the flight, even if it has a smaller influence on the flight holdup than the discharging rate.

Lee and Sheehan [28] compared the prediction of a geometric flight unloading model for a two-segments flight with experimental data. Using a high-speed camera, the authors measured the mean surface angle of the solid in the flight and ran their model with this value. The comparison of flight discharging rate shows quite a good agreement between experiment and model prediction. Model accuracy is highly dependent on an accurate measurement of the mean surface angle of the materials. Moreover, image analysis showed that, under some conditions, the unloading process is discontinuous and that the surface angle of the material is not constant during the unloading process.

Sunkara and co-workers [29] derived a geometric model for rectangular shaped flights to predict flight holdup and discharging rate. They investigated the influence of the flight length ratio on the dynamic

angle, the flight holdup and the cascading rate of the flight. They showed that the flight length ratio, in the studied range, has no influence on the dynamic angle while it greatly influences flight holdup and discharging rate. High initial cascading rates were observed at small flight length ratios, but the range of discharging angles was shorter than it was at high flight length ratios. They compared their model prediction with experimental results and showed that good agreement is observed. This model was then extended [8] to estimate the total particle surface area of the curtains using a geometrical approach of the curtain height. This work is limited to flights with 2 segments with an angle of 90° between them.

All previous studies have illustrated that dryer flights, and more specifically their design, are critical elements to consider when designing a rotating dryer. Indeed they can significantly influence the drying performance. Globally, to promote gas-solid contact, the particulate solids should rain over a large angle range or rotation [27].

This paper aims to further develop previous studies performed in the field of optimal flight design. Using a geometrical model like Revol [27] and Sunkara [29], we extend previous works by investigating the interaction of material with two segmented flight shape of arbitrary angle between segments. As in previous works, the influence of air flow is not considered here. More specifically, we investigate the flight holdup, the discharging angle range and the falling height by varying segment length ratio, the angle between these segments and the connecting angle of the flight with the drum wall. Influence of size ratio between flight segments and drum radius is also investigated. The paper is organised as follows. In the first part, we present the geometrical model and its assumptions. Then, we validate this model with an experimental set-up allowing us to measure the volume of material in flights using image analysis. Predictions of our model are then compared with experimental results obtained in this work and also with ones found in the literature. Finally, an analysis of the optimal flight shape is conducted and conclusions of this work are given.

2. Geometrical model

We consider a drum of radius R and length L with N_f identical flights as described in Fig. 1. The drum rotates at angular velocity w . The flight angular position is denoted θ whereas the angular position of flight tip is noted δ . Distance between a flight extremity and the cylinder axis in a

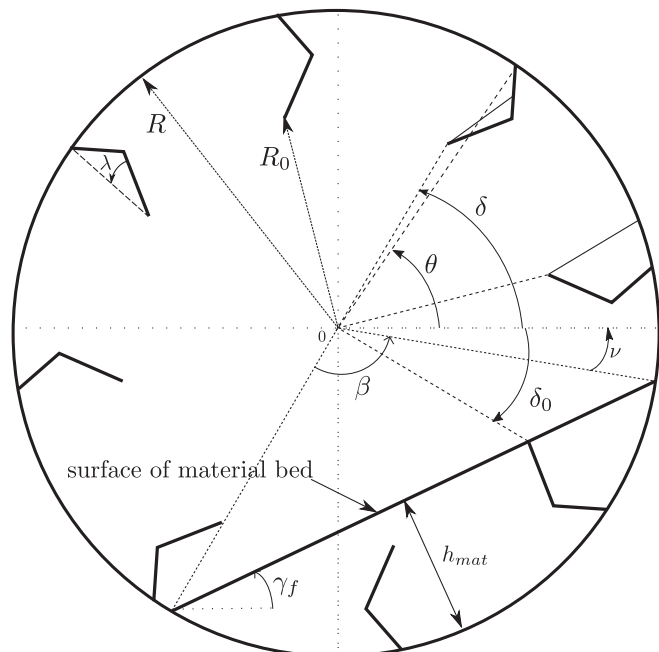


Fig. 1. Schematic view of the drum section with flights.

cross section (i.e the radius of the circle described by the flight tip) is R_0 .

2.1. Volume of material at the bottom of the drum

In this paper, the material inside the drum is a granular material which will be considered as a continuous medium. Therefore, the paper results may apply to granular materials for which the particle size is relatively small compared to the radius of the drum or the length of the flight segments.

The drum is partially filled with material with repose angle $\gamma_f = \text{atan}(\mu)$, where μ is the kinematic friction angle. The drum filling ratio is defined as: $\chi = \frac{V_{\text{material}}}{\pi R^2 L} = \frac{S_{\text{material}}}{\pi R^2}$, where V_{material} and S_{material} are respectively the volume occupied by the material and the cross-sectional area of the material. The relation between angle β (see Fig. 1) and χ is given by:

$$\chi = \frac{1}{2\pi}(\beta - \sin\beta) \quad (1)$$

The maximum height of material at the bottom of the drum, measured perpendicularly to the material surface, is $h_{\text{mat}} = R(1 - \cos\frac{\beta}{2})$.

It exists three different states of the drum loading that can be observed according to the position of the flight when it starts to discharge [22,30]. If the flight starts to discharge when it is in the upper half of the drum, it is said to be under-loaded. In this case, time spent by material in the airborne phase is quite reduced. It has been suggested that a dryer is operating in an under-loaded condition when the flights are not filled to their full capacity. If the drum loading increases, then flight starts to discharge sooner. The drum is said to be design-loaded when the unloading of the flight begins at $\delta = 0^\circ$. In design-loaded case, it is widely assumed that the amount of material in the airborne phase is maximum [22]. If the filling ratio of the drum is further increased, the drum is classified as over-loaded. There are more solids than required to completely fill the flight. In such case, the flight begins to discharge when it disengages from the material bed at an angle δ_0 . Nevertheless the volume of material carried-up by the flight is not increased. It is admitted that when $\delta < 0$, material falling from the flight directly roll on the material bed and therefore do not contribute to amount of material in the airborne phase. In this paper, as in the work of Sunkara et al. [8], we assume that the drum operates in either design or over-loaded conditions in a sense that flight is loaded at its full capacity (i.e $(R - R_0) \leq h_{\text{mat}}$). Due to the drum revolution, flights pass through the material bed and load a quantity of material. A flight disengages from the solid bed at an angle δ_0 when its extremity leaves the material bed (see Fig. 1):

$$\delta_0 = -\left(\frac{\pi}{2} - \gamma_f - \arccos\left(\frac{R\cos\frac{\delta_0}{2}}{R_0}\right)\right) \quad (2)$$

The corresponding angular position of the flight is denoted $\theta_0 = \theta_{\delta=\delta_0}$. Due to previous considerations, we assume that a flight begins to discharge and releases material in the airborne phase when the position of the flight extremity is $\delta = 0$. The corresponding value of θ will be denoted $\theta'_0 = \theta_{\delta=0}$

2.2. Volume of material in segmented flights

We consider a flight as described in Fig. 2.

It is composed of two segments of length l_1 and l_2 . The first segment forms an angle α_1 with the drum wall. Angle between the two segments is α_2 . The distance between flight extremity (point C) and cylinder axis (i.e. radius of the circle described by the tip of the flight) is given by:

$$R_0 = \sqrt{R^2 + l_1^2 + l_2^2 + 2R(l_2\sin(\alpha_1 + \alpha_2) - l_1\sin\alpha_1) - 2l_1l_2\cos\alpha_2} \quad (3)$$

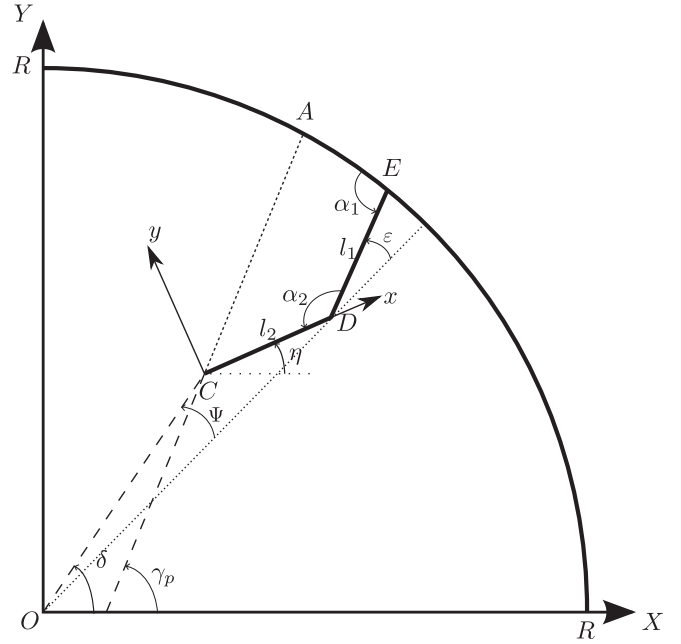


Fig. 2. Design of the two segmented flight studied in this paper.

The angular position of the flight tip is:

$$\delta = \theta + \arcsin\left[-\frac{1}{R_0}l_2\cos(\alpha_2 + \alpha_1) + l_1\cos(\alpha_1)\right] \quad (4)$$

The volume of material in lifters is a function of both the geometry of the lifter and the position of that lifter θ . It also depends on the angle of repose of the material and the filling ratio χ of the dryer. As said previously, we assume that the value of χ is sufficient to guarantee that all flights will be loaded at their full capacity.

By balancing forces acting on the volume of material transported by a flight, Schofield and Glikin [6] showed that the dynamic repose angle γ_p can be estimated with:

$$\tan\gamma_p = \frac{\mu + R_0\frac{w^2}{g}(\cos\delta - \mu\sin\delta)}{1 - R_0\frac{w^2}{g}(\sin\delta + \mu\cos\delta)} \quad (5)$$

Eq. (5) is widely accepted in literature [23,26,27,29]. It has been reported to be valid up to Froude number $Fr = \frac{w^2 R}{g} = 0.4$ [31]. It should be noted that in the range of operating parameters that will be used in

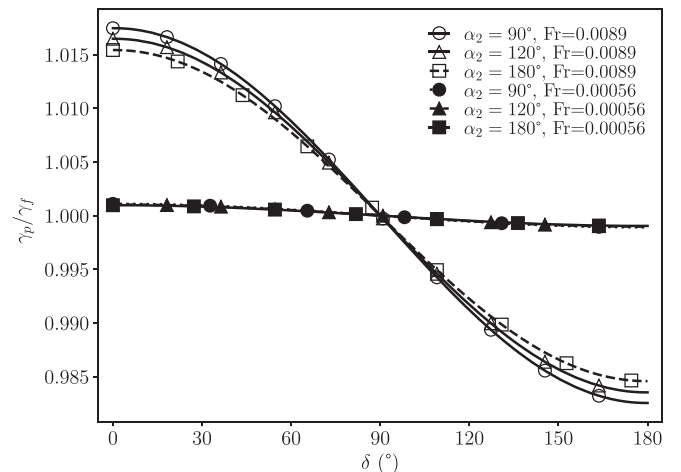


Fig. 3. γ_p/γ_f versus δ , for various α_2 , $\alpha_1 = 90^\circ$, $R/l_1 = 10$, $R = 0.5$ m, $l_2/l_1 = 1$ and $w = 1$ rpm ($Fr = 0.00056$) and $w = 4$ rpm ($Fr = 0.0089$).

this paper, the variation between γ_p and γ_f remains quite small. Fig. 3 shows indeed the evolution of γ_p/γ_f with δ for different Froude number values and α_2 . The values of Fr correspond respectively to $w = 1$ rpm and 4 rpm for $R = 0.5$ m. Fig. 3 shows that the influence of α_2 on γ_p remains quite small, especially for the value of angular velocity that will be used in this work ($Fr = 0.00056$).

The coordinates of points D and E in the local frame are expressed as:

$$x_D = l_2; y_D = 0 \quad (6)$$

$$x_E = x_D - l_1 \cos \alpha_2; y_E = l_1 \sin \alpha_2 \quad (7)$$

These coordinates are related to angles δ and η by the following relations:

$$x_E = R \cos(\theta - \eta) - R_0 \cos(\delta - \eta) \quad (9)$$

$$y_E = R \sin(\theta - \eta) - R_0 \sin(\delta - \eta) \quad (10)$$

The angle η between the local and global frames can be determined by solving equations (9) and (10). The surface position of the material contained in flight is given by $y = x \tan(\gamma_p - \eta)$. To determine the volume of material in a flight, we first need to calculate coordinates of intersection between material surface and the drum wall or a flight segment depending on whether the material is in contact with the drum wall or with a flight segment:

- the material comes in contact with the drum wall if $\gamma_p - \eta > \arctan\left(\frac{y_E}{x_E}\right)$. Intersection coordinates are found by solving the following equation

$$(X_A - X_C)^2 + (Y_A - Y_C)^2 = x_A^2(1 + \tan^2(\gamma_p - \eta)) \quad (11)$$

which leads to:

$$x_A = \frac{-B_A \pm \sqrt{B_A^2 - 4A_A C_A}}{2A_A} \quad (12)$$

with $A_A = 1 + \tan^2(\gamma_p - \eta)$, $B_A = 2X_C(\cos \eta - \tan(\gamma_p - \eta) \sin \eta) + 2Y_C(\tan(\gamma_p - \eta) \cos \eta + \sin \eta)$. Among these two solutions, we retain the one that satisfies:

$$y_A = x_A \tan(\gamma_p - \eta) > 0 \quad (13)$$

The cross sectional area occupied by the material in the flight is:

$$A_F = \frac{R^2}{2}(\kappa - \sin \kappa) + \frac{1}{2}(x_D y_E + y_A x_E - x_A y_E) \quad (14)$$

$$\text{where } \kappa = 2 \arcsin\left(\frac{\sqrt{(x_E - x_A)^2 + (y_E - y_A)^2}}{2R}\right).$$

- the material comes in contact with the first segment DE at coordinates (x_1, y_1) , if $\gamma_p - \eta < \arctan\left(\frac{y_E}{x_E}\right)$ and $\sqrt{(x_1 - x_E)^2 + (y_1 - y_E)^2} < l_1$. If $\alpha_2 \neq \frac{\pi}{2}$, then:

$$x_1 = \frac{-\tan(\alpha_2)l_2}{\tan(\gamma_p - \eta) + \tan \alpha_2} \quad (15)$$

$$y_1 = -(x_1 - l_2) \tan \alpha_2 \quad (16)$$

Else, if $\alpha_2 = \frac{\pi}{2}$, intersection coordinates are given by $x_1 = x_D = l_2$ and $y_1 = \tan(\gamma_p - \eta)x_D$.

The cross sectional area occupied by the material is:

$$A_F = \frac{1}{2}x_D y_1 \quad (17)$$

2.3. Maximum discharging angle of flight δ_{max}

As illustrated in Fig. 4, δ_{max} corresponds to the flight tip position where all material has left the flight. The corresponding flight position will be noted θ_{max} . Contrary to δ_0 , it is not possible to determine analytically values of δ_{max} for all flight configurations, since it depends on the dynamic repose angle γ_p given by equation (5), which in turn depends on δ (and so on δ_{max}). Maximum discharging angle δ_{max} is given by:

$$\delta_{max} = \pi + \gamma_p - \alpha_2 + \Psi - \varepsilon \quad (18)$$

where Ψ and ε are angles illustrated in Fig. 2 and given respectively by:

$$\Psi = \arctan\left(\frac{\frac{l_2}{l_1} \sin(\alpha_2 + \varepsilon)}{\frac{l_2}{l_1} \cos(\alpha_2 + \varepsilon) + \sqrt{\frac{R^2}{l_1^2} - 2\frac{R}{l_1} \sin \alpha_1 + 1}}\right) \quad (19)$$

$$\varepsilon = -\arcsin\left(\frac{\frac{R}{l_1} \cos \alpha_1}{\sqrt{\frac{R^2}{l_1^2} - 2\frac{R}{l_1} \sin \alpha_1 + 1}}\right) \quad (20)$$

To obtain the maximum discharging angle, we can numerically solve equation (18).

2.4. Falling height of material

Assuming a vertical fall of material, we can calculate the falling height of solid leaving the flight according to the angular position of the flight. It has been shown that such an assumption is reasonable [8,32] and that it deviates from experimental results only for high Froude numbers due to the dispersion of the curtains in such a case [8]. This will

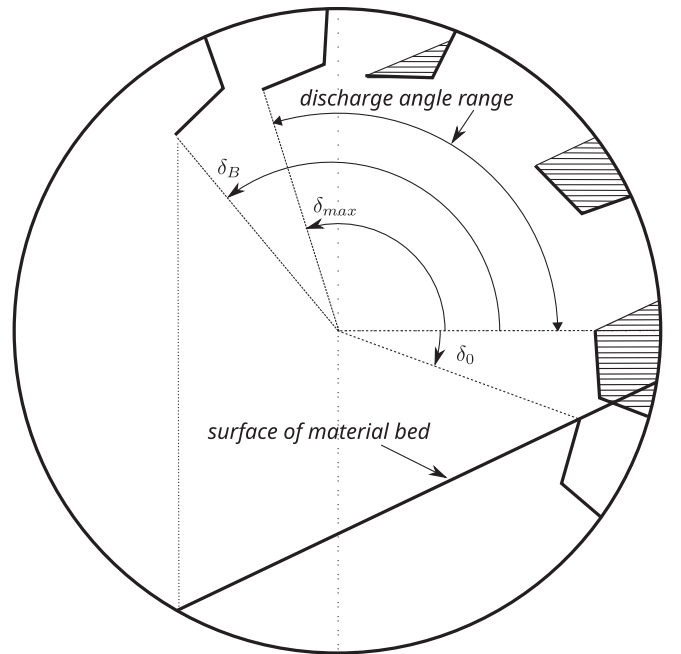


Fig. 4. Schematic view of angles δ_0 , δ_{max} and δ_B . The flight leaves the material bed at $\delta = \delta_0$, it starts to discharge at angle $\delta = 0^\circ$ and is completely empty at angle δ_{max} , angle which can be smaller or larger than δ_B . Material leaving the flight can impact the material bed from $\delta = 0^\circ$ to $\delta \leq \delta_B$.

be illustrated in part 3 during validation of the model. Depending on the angular position δ , the drum filling ratio χ and the material repose angle γ_f , particles leaving the flight can impact on the material bed at the bottom of the drum, on the drum wall or on another flight. Impact on other flights is rather complex to estimate particularly for flight geometries investigated in this paper. Moreover its influence acts only for large values of discharging angle and therefore on a small amount of material. For these reasons, interactions of material with flights are not considered in this work.

The falling material impacts the material bed for $0 < \delta < \delta_B$ where δ_B is the maximum angle for which a particle of the granular material leaving the flight can fall on the material bed located at the bottom of the drum, as described in Fig. 4.

$$\delta_B = \pi - \arccos\left(\frac{R}{R_0}\sin\left(\frac{\beta}{2} - \gamma_f\right)\right) \quad (21)$$

Depending on the volume carried up by the flight, the material properties and the drum filling ratio, it is important to note that the maximum discharging angle of the flight δ_{max} can be smaller or larger than δ_B . This means that for certain configurations, the material leaving the flight only interacts with material bed at the bottom of the drum.

In this case ($0 < \delta < \min[\delta_B, \delta_{max}]$), the falling height of the material is given by:

$$\begin{aligned} \frac{h_f}{R} &= \frac{R_0}{R}(\sin\delta - \cos\delta\tan\gamma_f) + \sin(\beta + \nu) + \cos(\beta + \nu)\tan\gamma_f \\ &= \frac{\cos\frac{\beta}{2}}{\cos\gamma_f} + \frac{R_0}{R}(\sin\delta - \cos\delta\tan\gamma_f) \end{aligned} \quad (22)$$

If $\delta > \delta_B$ and if the flight continues to discharge itself, material leaving the flight interacts with the drum periphery. In this case, the falling height is:

$$\frac{h_f}{R} = \frac{R_0}{R}\sin\delta - \sqrt{1 - \left(\frac{R_0}{R}\right)^2 \cos^2\delta} \quad (23)$$

2.5. Maximum number of flights

The number of flights in a rotary dryer should generally be as large as possible, in order to maximise the holdup and make the most effective use of the dryer volume [24]. For $\delta = 0$, the corresponding flight is fully charged and the material comes in contact with the drum wall at point A. The maximum number of flights along the drum wall is directly related to the coordinates (X_A, Y_A) of this point as described in Fig. 5. However, the optimum number of flights should guarantee that the top surface material in a flight should not intercept other flights.

Therefore, maximum number of flights N_{fmax} can be safely estimated through:

$$N_{fmax} = \text{floor}\left(2\pi \left[\arctan\left(\frac{Y_A}{X_A}\right) - \min_{\delta=\delta_0} \left[\delta; \arctan\left(\frac{Y_D}{X_D}\right); \theta \right] \right]_{\delta=0} \right)^{-1} \quad (24)$$

While the maximum number of flights N_{fmax} can be determined with Eq. (24), the number of active flights N_{fa} can be expressed as: $N_{fa} = N_{fmax} \times \delta_{max}/(2\pi)$.

2.6. Model implementation

Equations of this geometrical model have been implemented into a numerical program to simulate the holdup and discharge of material in the drum with N_p flights rotating with speed w . This drum contains a granular material of repose angle γ_f up to a drum filling ratio of χ . It allows us to investigate the optimal flight shape by varying the angle α_2 between the flight segments, the flight connecting angle α_1 , the length of each segment (l_1 and l_2), the maximum number of flights and the drum radius.

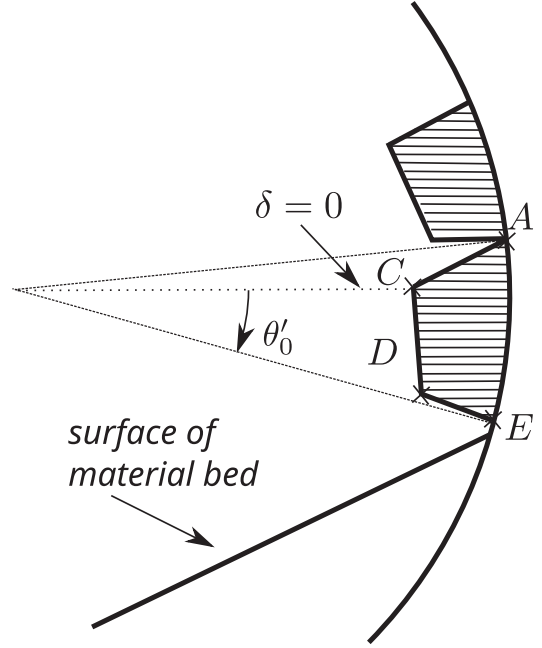


Fig. 5. Schematic view of optimal flight loading.

2.7. Analysis of optimal flight shape

Following analysis of Sunkara et al. [8] we have assumed a 2D model, thus the flight has the same length L as the drum. Therefore, the volume of material in a flight i with angular position θ is

$$V_{F_i}(\theta) = A_{F_i}(\theta)L \quad (25)$$

where $A_{F_i}(\theta)$ is the cross-sectional area occupied by the material in the flight. We can define $f_{F_i}(\theta)$ as the ratio between the volume of material in flight i and the total volume of the drum.

$$f_{F_i}(\theta) = \frac{A_{F_i}(\theta)}{\pi R^2} = \frac{m_{F_i}(\theta)}{\rho_b \pi R^2 L} \quad (26)$$

f_{F_i} will be referred as the filling degree of the flight representing the volume of material in the flight per unit volume of the drum. m_{F_i} and ρ_b are respectively the mass of material in flight i at angular position θ and the density of the bulk of the material. The mass of the material in flight is expressed as $m_{F_i}(\theta) = \rho_b \pi R^2 L f_{F_i}(\theta)$. When the flight moves from $d\theta$, the cascading rate of material released by this flight in the air stream can be expressed as:

$$\frac{d(m_{F_i}(\theta))}{dt} = w \rho_b \pi R^2 L \frac{df_{F_i}(\theta)}{d\theta} \quad (27)$$

The dimensionless cascading rate $c_i(\theta) = \frac{-df_{F_i}(\theta)}{d\theta}$ is the dimensionless volume of particles (i.e the number of particles) leaving flight i per unit of angle. To optimise the drying of a material, it is important to try to maximise the surface of exchange between hot gas and solid material. For this reason, we should consider the local transfer area A_{C_i} of curtain i which can be seen as the number of particles of granular material in curtain i multiplied by the exchange surface of a particle [8]. Therefore we have:

$$A_{C_i}(\theta) = \frac{6m_{C_i}(\theta)}{\rho_s d_p} \quad (28)$$

where $m_{C_i}(\theta)$ is the mass of material in curtain i when flight is at angular position θ , d_p and ρ_s are respectively the diameter of granular material particles and the density of the particles. Using the vertical free fall assumption, the time of fall between the flight extremity and the impact

point, which can be considered as the retention time in the hot air stream, is [33]:

$$t_f(\theta) = \frac{1}{w} \sqrt{2Fr \frac{h_f(\theta)}{R}} \quad (29)$$

h_f is the falling length given by Eqs. (22) and (23) depending on whether the falling material impacts the bed or the drum wall. Then, the filling degree of the curtain $f_{Ci}(\theta)$ is:

$$f_{Ci}(\theta) = \frac{m_{Ci}(\theta)}{\rho_b \pi R^2 L} = \sqrt{2Fr \frac{h_f(\theta)}{R}} c_i(\theta) \quad (30)$$

Eq. (28) becomes [8]:

$$\frac{A_{Ci}(\theta)}{LR} = 3\pi \left(\frac{\rho_b}{\rho_s} \right) \left(\frac{D}{d_p} \right) f_{Ci}(\theta) \quad (31)$$

Heat transfer due to lifting flights is directly related to the total particle surface area in all curtains [8,32,34]. An estimate of the dryer performance during a cascading cycle of one flight can therefore be achieved by considering summation of local transfer area A_{Ci} over a cascading cycle during one revolution of the drum.

$$G_{Ci} = \frac{1}{w} \int_{\theta'_0}^{\theta_{\max}} \frac{A_{Ci}(\theta)}{LR} d\theta = 3\pi \left(\frac{\rho_b}{\rho_s} \right) \left(\frac{D}{d_p} \right) G_{Ci}^* \quad (32)$$

with

$$G_{Ci}^* = \frac{1}{w} \int_{\theta'_0}^{\theta_{\max}} f_{Ci}(\theta) d\theta \quad (33)$$

Since all flights of the drum will contribute during one drum revolution, the total cumulative filling degree of the curtain, considering contributions of all drum flights distributed along its periphery, can be estimated by the product of G_{Ci} with the maximum number of flights. Thus:

$$\zeta_{\max} = N_{f \max} \times G_{Ci} = 3\pi \left(\frac{\rho_b}{\rho_s} \right) \left(\frac{D}{d_p} \right) \zeta_{\max}^*$$

, with $\zeta_{\max}^* = N_{f \max} \times G_{Ci}^*$. ζ_{\max} (or ζ_{\max}^*) can be assimilated to the cumulative transfer area of material carried by all flights during one drum revolution.

2.8. Discussions of the geometrical model approach

The model developed and presented in the previous sections is based on several assumptions. Despite the fact that they are quite reasonable, it is therefore important to emphasise them in order to understand the limitations and possible further developments of this model. The first assumption is that the material is a non-cohesive granular material with a dynamic repose angle given by Eq. (5). The material transported by a flight or located in the bed is considered to be a continuous medium. For this reason, as said previously, we assumed that the size of the particles constituting the granular material is relatively small compared to the drum radius and the length of flight segments. This allowed us to consider a flat surface material in bed and in each flight (segment AC in Fig. 2) respectively through Eqs. (1) and (13). Moreover, we assume that all particles are spherical.

Heat transfer is not addressed in this work. Nevertheless, as a first step to a more complex model that would include heat transfer, it can be interesting to analyse the influence of the assumptions made in this work. Heat transfer is usually analysed in terms of a volumetric heat transfer coefficient, which can be estimated or derived from the effective surface area of the particles in contact with the gas stream [34,35]. In this work, this surface, also called curtain area, is determined using the retention time of particles in the curtain [34] based on the assumption of vertical free fall of particles from the flight tips. Particles can fall on the

material bed or on the drum wall but the falling of material on the flights located out of the granular material bed is not considered in this work. Moreover we neglect the shielding effect of particles. This last one would tend to reduce the heat transfer coefficient. Since drag and lift forces are also not taken into account, their incorporation in such a model would increase falling time of particles which in turn would enlarge surface material in airborne phase in contact with air stream. This would lead to an increase of the heat transfer coefficient. However, if the temperature could not be considered as uniform over the entire drum cross section, the gas near curtains with high particle concentration would have lower temperature.

As the distribution of particles along drum axis is considered as uniform, the application of the model is limited to a cross section. The drum is assumed to be either design-loaded or over-loaded in a sense that a flight is loaded at its maximum capacity when it leaves the material bed. Moreover, due to the cyclical aspect of the loading and unloading phases during rotation of the drum, the volume of material inside the bed is kept constant during rotation cycle. This can be assimilated to a rotary dryer continuously supplied with material.

3. Model validation with experiment

In our knowledge, all experiments available in the literature, with two-segmented flights, report results with angles α_1 and α_2 of 90° [8,29]. No other angle has been studied especially for discharging profile. Some works have been done numerically [14], but not for particles that were small enough to consider the material surface as flat. To validate our geometrical model and also the validity of the assumptions described previously in Section 2.8, we developed an experimental set-up to measure the volume of material carried up by two-segmented flights with different values of α_2 and ratio l_2/l_1 .

The experimental device consists of a rotating cylinder of radius $R = 0.15$ m made of polyvinyl chloride. Length of cylinder accessible to material is 0.04 m and it can be closed with a plexiglass cover. Polylactic acid (PLA) flights can be placed on the inner circumference of the drum. In this work, in order to validate the model for one flight, we only use one flight. Acquisition is made using a video camera coupled with a triggering device at a framerate of 50 Hz.

To analyse images obtained from the camera, as illustrated in Fig. 6, we developed a python code using opencv library [36]. This permits to determine the volume of material in a flight at different angular positions. Moreover the falling height of material is estimated using ImageJ software [37]. Different flight shapes have been tested: $\alpha_2 = 90^\circ$, $\alpha_2 = 120^\circ$, $\alpha_2 = 150^\circ$ and $\alpha_2 = 180^\circ$ and two values of the ratio $l_2/l_1 = 0.5, 1$. We use quartz sand of diameter $d = 0.6$ mm and $\gamma_f = 36^\circ$.

3.1. Flight holdup and discharging profiles

In a first step, we compared the flight holdup and the cascading rate predicted by our model with our experimental results and with ones obtained from literature [29]. Fig. 7 presents flight filling degree f_{Fi} with discharging angle δ predicted by the geometrical model. Different flight shapes, with different values of α_2 are presented.

In a same manner the predicted flight holdup for flights with different ratio l_2/l_1 is presented in Fig. 8. Both figures show a good agreement between prediction of the geometrical model and experimental results.

The measured values of the holdup were used to evaluate the rate of variation in the flight filling degree. We compute the cascading rate c_i as the opposite of the change in the flight filling degree over the corresponding change in the discharge angle. Fig. 9 presents c_i with δ for different values of l_2/l_1 and α_2 . Both experimental results and our model predictions are represented.

Figs. 7–9 show good agreement between the geometrical model and experimental data for different flight shapes (different ratios l_2/l_1 and different values of α_2). It can be concluded that the volume of material in

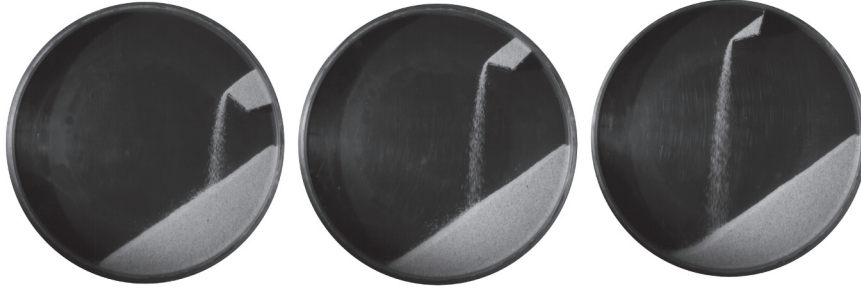


Fig. 6. Example of pictures of a flight discharge obtained with the experimental device, using quartz sand of diameter $d = 0.6$ mm.

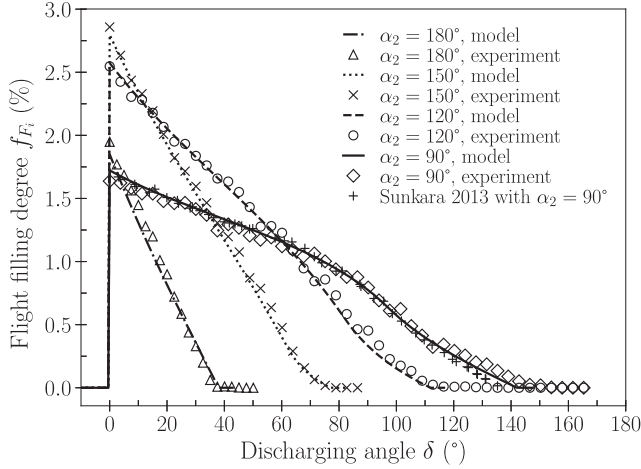


Fig. 7. Comparison of flight holdup predicted by the geometrical model with our experimental data for different α_2 ($R = 0.15$ m, $w = 1$ rpm, $\mu = \arctan(36^\circ)$) using quartz sand of diameter $d = 0.6$ mm) and results of Sunkara [29] ($R = 0.25$ m, $\alpha_2 = 90^\circ$, $\mu = \arctan(32.4^\circ)$) and $w = 2$ rpm, using quartz sand of diameter 0.2 mm) with $\alpha_1 = 90^\circ$, $R/l_1 = 5$, $l_2/l_1 = 1$ and $\chi = 15\%$.

flight and its discharge are correctly estimated with the geometrical model used in this work. Influences of α_2 and size ratio l_2/l_1 will be more precisely analysed in Section 4.1.

3.2. Falling height

Sunkara and co-workers [8] reported measurements of mean falling height of material over discharging angle range for two values of angular speed w . According to the authors, experimental data can be represented with 10% error bars. Nevertheless, as explained previously, these experiments were limited to flights with $\alpha_2 = 90^\circ$. We conducted a series of experiments to determine falling height of material for different values of α_2 . Length of particle trajectories were measured for different discharging angles. Errors were estimated using minimum and maximum values of trajectory lengths.

These results are presented in Fig. 10 in conjunction with the falling height predicted by the model and results of Sunkara et al. [8]. It can be observed in Fig. 10 that good agreement is obtained between model prediction and our experimental results, especially for values of discharging angles below 100° . Indeed, it is important to recall that one of the main assumptions of this model is that the falling trajectory is a vertical line, which is obviously not the case for a large discharging angle where granular material tends to hit the drum wall instead of falling straight down. Moreover, this also explains why predicted falling height is in the lower error range of our experiment. Fig. 10 also illustrates that predictions of our model deviate from results of Sunkara and co-workers [8] for discharging angles larger than 100° . Indeed, our

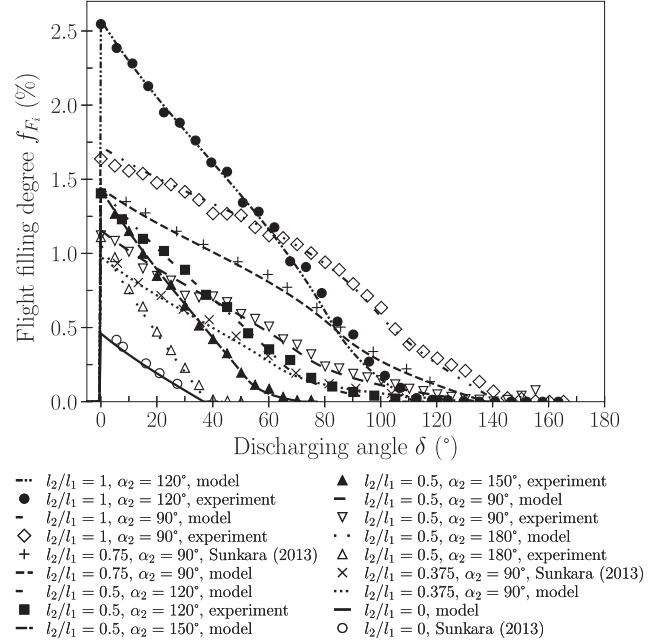


Fig. 8. Comparison of flight holdup predicted by the geometrical model, for different α_2 and l_2/l_1 ratio, with our experimental data ($R = 0.15$ m, $w = 1$ rpm, $\mu = \arctan(36^\circ)$) using quartz sand of diameter $d = 0.6$ mm) and results of Sunkara [29] ($R = 0.25$ m, $\alpha_2 = 90^\circ$, $\mu = \arctan(32.4^\circ)$) and $w = 2$ rpm ($Fr = 0.0011$), using quartz sand of diameter 0.2 mm) with $\alpha_1 = 90^\circ$, $R/l_1 = 5$ and $\chi = 15\%$.

model does not take into account the presence of other flights during the falling process. For this reason our experiments use only one flight which is not the case for experiments of [8]. This impact with other flights is more likely to occur for large δ . For these reason, we can state that our model can overestimate the falling height at the end of the discharging profile if the drum is equipped with several flights. Nevertheless, the amount of material involved is quite limited relatively to the total mass of material released in the curtain, since it occurs at the end of the flight discharge.

It can also be seen in Fig. 10 that the inertial effect, that increases with angular speed w , tends to increase experimental falling height while it has no effect on predictions of geometrical model with the vertical fall assumption. As also observed by Sunkara [8], this deviation is the result of a change in the trajectories of the curtains at higher Froude numbers.

To conclude, Fig. 10 illustrates that the falling height is correctly estimated with our model, despite the assumption of free vertical fall. Deviation with experimental data of [8] can be explained for large values of δ . Nevertheless, their effects can be considered as relatively negligible and since h_f will be used through the integration of curtain

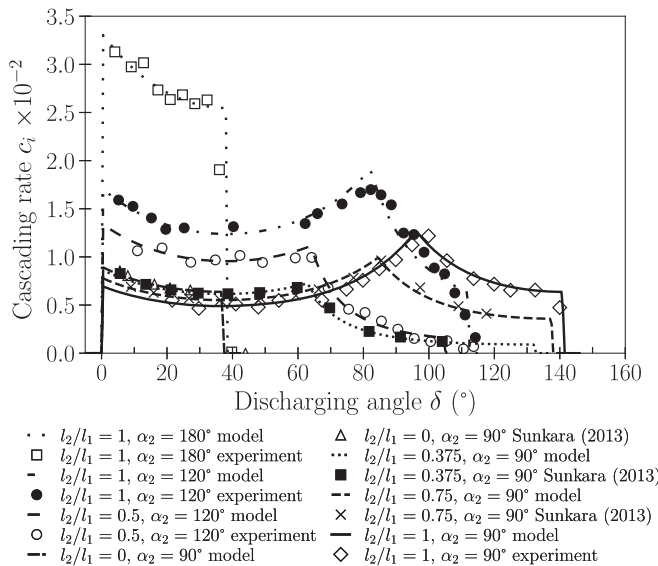


Fig. 9. Comparison of cascading rate predicted by the geometrical model, for different α_2 and l_2/l_1 ratio, with our experimental data ($R = 0.15$ m, $w = 1$ rpm, $\mu = \arctan(36^\circ)$) using quartz sand of diameter $d = 0.6$ mm) and results of Sunkara [29] ($R = 0.25$ m, $\alpha_2 = 90^\circ$, $\mu = \arctan(32.4^\circ)$) and $w = 2$ rpm ($Fr = 0.0011$), using quartz sand of diameter 0.2 mm with $\alpha_1 = 90^\circ$, $R/l_1 = 5$ and $\chi = 15\%$.

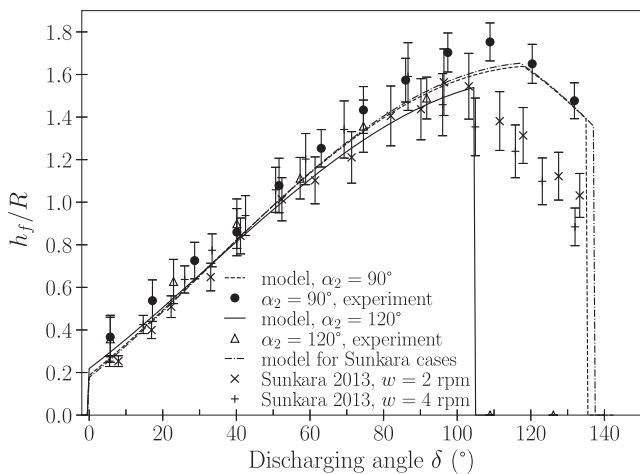


Fig. 10. Comparison of falling height predicted by the geometrical model with our experimental data ($R = 0.15$ m, $w = 1$ rpm, $\mu = \arctan(36^\circ)$) using quartz sand of diameter $d = 0.6$ mm) and results of Sunkara [29] ($R = 0.25$ m, $l_2/l_1 = 0.75$, $\alpha_2 = 90^\circ$, $\mu = \arctan(32.4^\circ)$), using quartz sand of diameter 0.2 mm with a drum equipped with 18 flights) with $\alpha_1 = 90^\circ$, $R/l_1 = 5$ and $\chi = 15\%$.

filling degree over discharging angle range, we can state that tendencies and results obtained in this work, even if they can be slightly overestimated, are correct.

4. Results

We have investigated the influence of the parameters of flight shape on the material holdup, the cascading rate and the dryer performance.

4.1. Influence of α_2 , l_2/l_1 and χ

First, we chose to investigate the case where the flights are attached perpendicularly to the wall ($\alpha_1 = 90^\circ$), since it is the most common case

[28]. We performed several calculations by varying the angle α_2 for $R/l_1 = 10$, $R = 0.5$ m, $l_2/l_1 = 1$, $\chi = 10\%$ and $\mu = 0.5$. The dependency of the flight filling degree f_{Fi} on α_2 is presented in Fig. 11. f_{Fi} is plotted against flight tip angular position δ . As expected, as flight discharges itself, f_{Fi} decreases with δ .

Moreover Fig. 11 shows that the angle between the two flight segments has important influence on the discharging profile of the flight. It should be noted that the initial volume of material in a flight $f_{Fi_{max}}$ also depends on the angle between the segments. Fig. 12 represents maximum filling degree $f_{Fi_{max}}$ of the flight as a function of α_2 such as $l_2/l_1 = 0.5, 1, 1.5, 2$, $\chi = 10\%$, $R/l_1 = 10$ and $R = 0.5$ m. On the whole, we can observe that $f_{Fi_{max}}$ increases with l_2/l_1 and with α_2 except for large values of α_2 (greater than 140°). This behaviour is expected since the volume of material in flight is determined by the line inclined at angle γ_p and passing through the flight extremity (segment AC in Fig. 2) [7].

It can be observed that the maximum flight filling degree is obtained with angle α_2 between 120° and 160° . This figure also illustrates that the angle α_2 which allows the maximum flight filling degree tends to increase with the ratio l_2/l_1 .

Fig. 13 shows the variation of the cascading rate c_i in the range of α_2 $60^\circ - 180^\circ$ when the flight shape is described by $l_2/l_1 = 1$, $R/l_1 = 10$, $\alpha_1 = 90^\circ$ and the drum of radius $R = 0.5$ m is filled with $\chi = 10\%$. This figure illustrates the fact that c_i can be considered as quite uniform over the discharging angle range only for $60^\circ < \alpha_2 < 90^\circ$. Moreover, the uniformity of the release of particles from the flight decreases when α_2 increases, and cascading rate becomes more important for small values of discharging angle δ . Particles leave the flight more quickly when the two segments tend to be aligned ($\alpha_2 = 180^\circ$). Material lost by a flight and released in the curtain, during a variation of angle δ , is approximately proportional to the length of the line AC (see Fig. 2) [7]. This explains the variation of c_i with α_2 illustrated by Fig. 13. Indeed, during the discharging of the flight, the length of AC decreases until $\delta = \gamma_p$, then it increases until the point A is superimposed with point E. In this case the cascading rate has reached its maximum value occurring at $\delta = \pi - (\lambda + \varepsilon + \alpha_2 - \gamma_p - \psi)$ depending particularly on α_2 . After this angle, the length of AC, hence the cascading rate, decreases continuously.

It can be interesting to consider variation of δ_0 with α_2 . Fig. 14 illustrates that the angle δ_0 , for which the flight disengages from the bed, decreases with α_2 and increases with χ . Nevertheless, as explained before, the flight is assumed to release material in the curtain at an angle $\delta = 0^\circ$ which does not depend on α_2 nor χ . The dependency for different values of l_2/l_1 are also presented in Fig. 14. Dependency of the terminal discharge angle of a flight δ_{max} on α_2 is illustrated in Fig. 15.

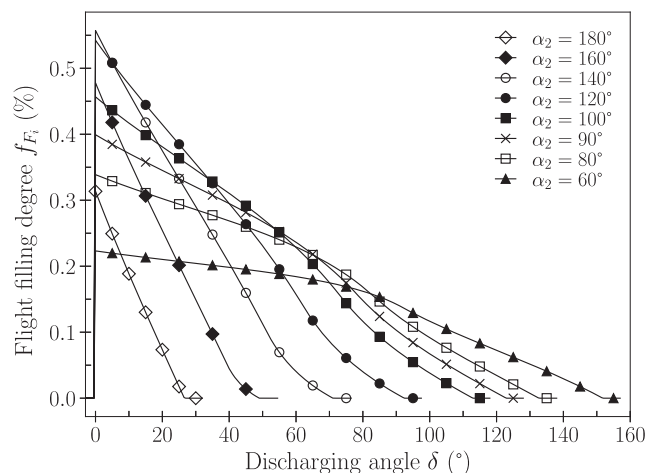


Fig. 11. Flight filling degree with discharging angle obtained for $l_2/l_1 = 1$, $R/l_1 = 10$, $R = 0.5$ m, $w = 1$ rpm, $\mu = 0.5$, $\alpha_1 = 90^\circ$, various α_2 and $\chi = 10\%$.

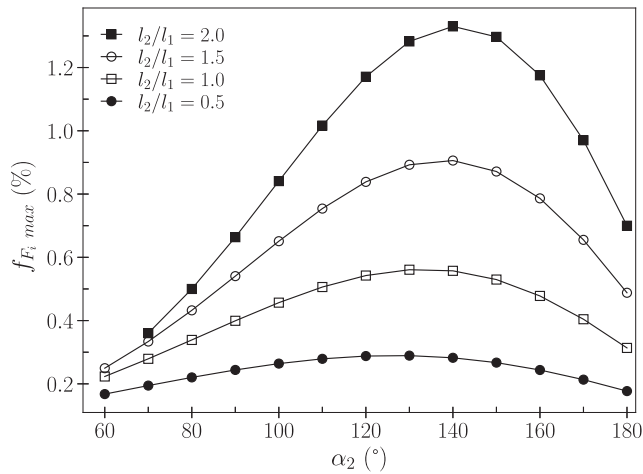


Fig. 12. Maximum flight filling degree with α_2 obtained for $l_2/l_1 = 1$, $R/l_1 = 10$, $R = 0.5$ m, $w = 1$ rpm, $\mu = 0.5$, $\alpha_1 = 90^\circ$ and $\chi = 10\%$.

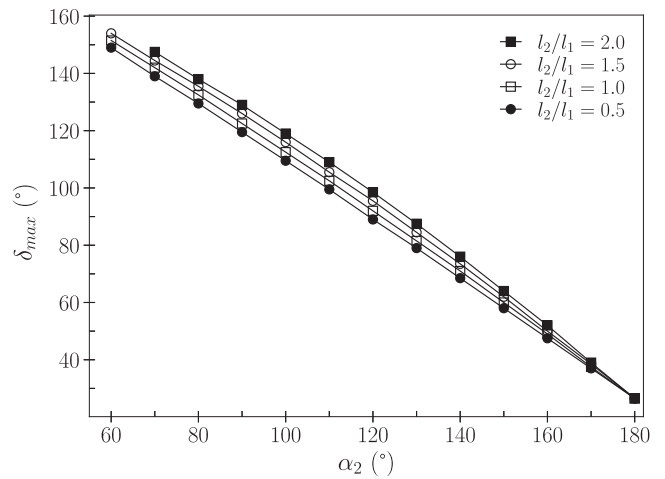


Fig. 15. Maximum discharging angle with α_2 obtained for various l_2/l_1 and for $\alpha_1 = 90^\circ$, $\chi = 10\%$, $R/l_1 = 10$, $R = 0.5$ m, $w = 1$ rpm, and $\mu = 0.5$.

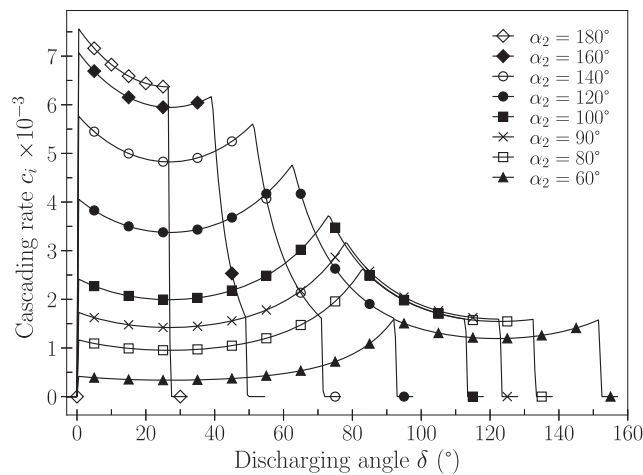


Fig. 13. Cascading rate with discharging angle obtained for $l_2/l_1 = 1$, $R/l_1 = 10$, $R = 0.5$ m, $w = 1$ rpm, $\mu = 0.5$, $\alpha_1 = 90^\circ$, $\chi = 10\%$ and various α_2 .

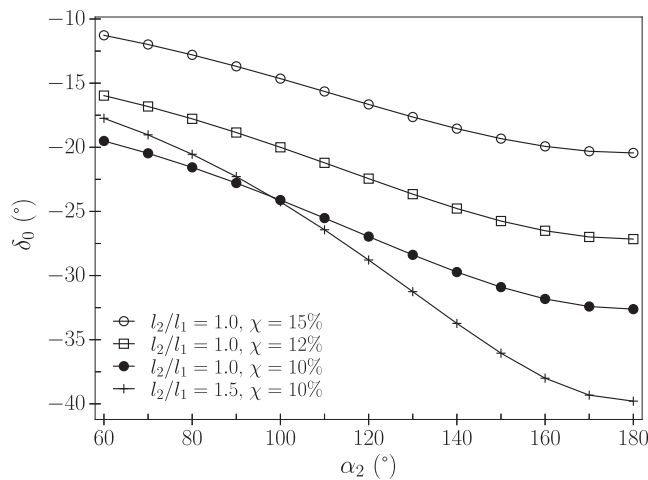


Fig. 14. Angle for which the flight disengages from the material bed with α_2 obtained for various l_2/l_1 , $\alpha_1 = 90^\circ$ and various χ with $R/l_1 = 10$, $R = 0.5$ m, $w = 1$ rpm, $\mu = 0.5$.

Fig. 15 shows clearly that δ_{max} almost “linearly” decreases when α_2 increases from 60° to 180° . This can be explained by considering Eq. (18). Given a α_1 value, ε is fixed. When varying α_2 , variations of ψ remain small (at maximum 6.34° in our case). So if we define a constant $k = \pi - \varepsilon$, Eq. (18) leads to $\delta_{max} = k + \psi + \gamma_p - \alpha_2$. Since variations of γ_p around γ_f remain small, δ_{max} can be roughly estimated with $\delta_{max} \approx k + \psi + \gamma_f - \alpha_2$, where ψ and ε are given by Eqs. (19) and (20).

Variation range of δ_{max} is quite important (from 30° to 160°), which clearly illustrates that flight discharging angle range increases significantly when the position of flight extremity tends to be higher (lower value of α_2). It can also be noted that even if δ_{max} increases with the aspect ratio l_2/l_1 , it does not play an important role to increase δ_{max} compared to α_2 . Since flight is loaded at its full capacity, δ_{max} is obviously not dependent on χ .

The falling height of the particles is a quantity which deserves to be checked in order to improve the dryer performance. For example, the filling degree of the curtain depends on the rate of material released by the flight and also on the falling height h_f given by Eqs. (22) or (23). Thus it depends on the angle δ and the filling ratio χ . Fig. 16 illustrates evolution of h_f/R with discharging angle δ for different values of α_2 and drum filling ratio χ . It can be observed in Fig. 16 that obviously the falling height increases with the increase of the discharging angle, and that it tends to a limit at δ_{max} for which the flight is completely

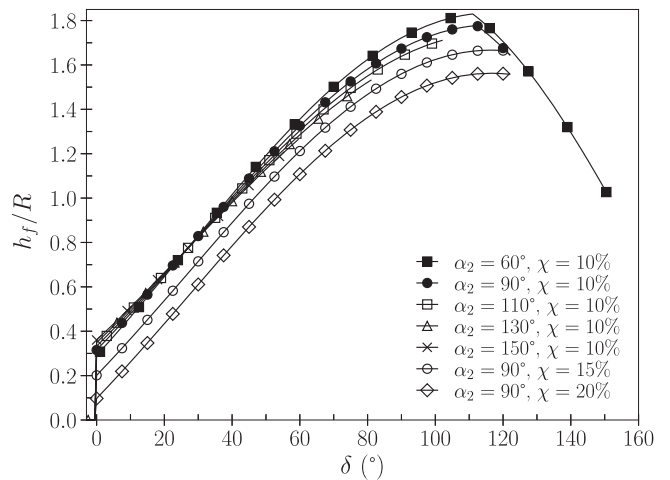


Fig. 16. Dimensionless falling height h_f/R with δ obtained for $l_2/l_1 = 1$, $R/l_1 = 10$, $R = 0.5$ m, $w = 1$ rpm, $\mu = 0.5$, $\alpha_1 = 90^\circ$ and various α_2 and χ .

discharged. However, for the case $\alpha_2 \leq 90^\circ$, the falling height decreases after it reaches a maximum because the remaining particles at this stage impact the drum wall in place of the material bed ($\delta_{max} > \delta_B$). As we might have expected, Fig. 16 illustrates that the falling height h_f decreases when the filling ratio of the drum increases. It can also be observed that for a given position δ , α_2 has less influence than χ on h_f/R .

Fig. 17 shows evolution of maximum curtain filling degree for $\chi = 10\%$, $\alpha_1 = 90^\circ$, as a function of angle α_2 for various l_2/l_1 ratio.

It increases with α_2 up to an optimal value of α_2 (between 140° and 170° for the l_2/l_1 range investigated), and then decreases. Moreover, the maximum curtain filling degree increases with ratio l_2/l_1 , since the volume carried and released by the flights also increases with this ratio.

The cumulative transfer area G_{Ci}^* (Eq. (33)) is a parameter that can provide useful indications to maximize the contact of particles with the hot air steam. Fig. 18 shows the evolution of G_{Ci}^* with α_2 for various ratio l_2/l_1 and χ values. We can observe that similarly to the evolution of the maximum curtain filling degree, cumulative curtain filling degree G_{Ci}^* increases, then decreases with α_2 . On the whole, G_{Ci}^* is larger when the length of the second flight segment l_2 increases. As previously observed in Fig. 12 and 16, this is more related to the increase in material volume lifted by the flight than to the increase of the falling height. Fig. 18 highlights that the optimum angle α_2 to maximize G_{Ci}^* is between 115° – 140° and increases with l_2/l_1 . As previously observed in Fig. 16, the drum filling ratio χ greatly reduces falling height h_f . For this reason, when considering the influence of χ on G_{Ci}^* , as presented in Fig. 18, we can notice that G_{Ci}^* decreases with increasing χ .

4.2. Influence of α_1

As said previously, in industries using rotary dryers, flights are usually fixed to the drum wall with an angle $\alpha_1 = 90^\circ$ [28]. This is mainly for practical reasons. However, wet granular materials are usually cohesive and a clogging of the flights can be encountered. We believe that, as a prevention of this phenomenon, we should choose a not so small angle depending on material. Nevertheless, with a cohesionless material, as it is assumed in this study, what is exactly the influence of α_1 on the curtain filling degree? To investigate this, we have conducted a series of computations for flights fixed to the drum wall with different values of α_1 and for all the range of angle α_2 previously studied. The dependency of G_{Ci}^* on α_2 for different angles α_1 is presented in Fig. 19.

It shows that the maximum of G_{Ci}^* is obtained with α_1 in the range

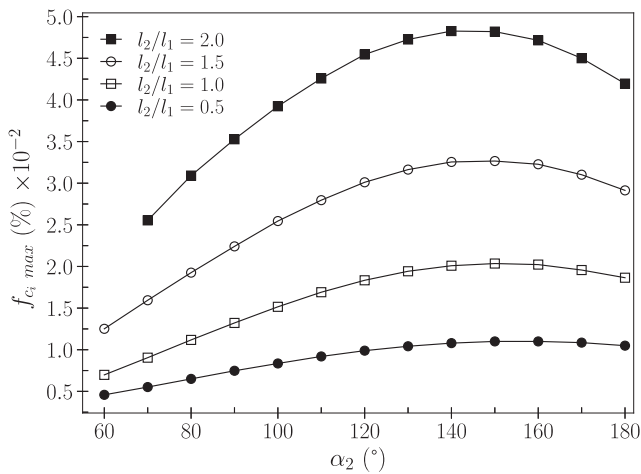


Fig. 17. Maximum filling degree of the curtain with α_2 obtained for various values of l_2/l_1 , $R/l_1 = 10$, $R = 0.5$ m, $w = 1$ rpm, $\mu = 0.5$, $\alpha_1 = 90^\circ$ and $\chi = 10\%$.

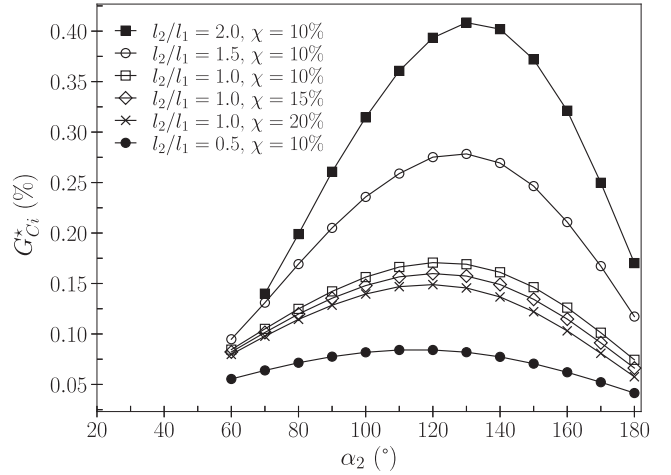


Fig. 18. Cumulative curtain filling degree during one cascading cycle with α_2 obtained for various l_2/l_1 and χ , $R/l_1 = 10$, $R = 0.5$ m, $w = 1$ rpm, $\mu = 0.5$, $\alpha_1 = 90^\circ$.

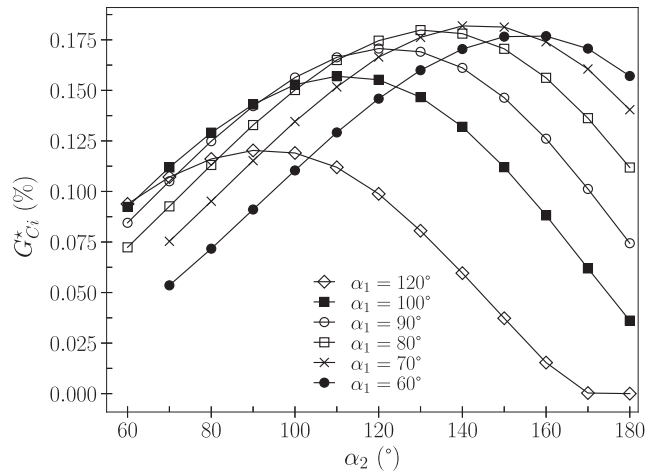


Fig. 19. Cumulative curtain filling ratio during one cascading cycle with α_2 obtained for various value of α_1 , $l_2/l_1 = 1$ with, $R/l_1 = 10$, $R = 0.5$ m, $w = 1$ rpm, $\mu = 0.5$ and $\chi = 10\%$.

70° – 80° . This maximum decreases when α_1 increases. From a global point of view, the maximum of the cumulative curtain filling can be obtained for α_1 around 80° . When $\alpha_1 \leq 100^\circ$, a relative high value of G_{Ci}^* can be obtained for $110^\circ \leq \alpha_2 \leq 140^\circ$. Results presented in Fig. 19 show that if we need to slightly increase α_1 to reduce clogging for a particular product, this can be accompanied with a decrease of α_2 to maintain a quite large value of G_{Ci}^* .

4.3. Number of flights

In this section, we investigate the maximum number of identical flights which it is possible to distribute along the drum periphery for each configuration. In practice, it is not easy and not often desired to change the lifting layout of a drum dryer every time the material or operational conditions are changed. For a specific drum, if we know the number of flights and their shapes, it is possible to estimate the dryer performance of the drum by multiplying F_{Ci} by the number of flights in the drum.

Fig. 20 shows the evolution of the maximum number of flights given by Eq. (24) with α_2 . On the whole, we observe that when

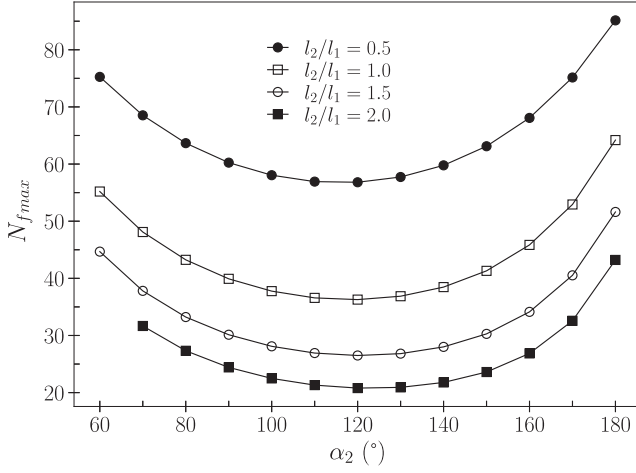


Fig. 20. Maximum number of flights with α_2 for various l_2/l_1 with $\alpha_1 = 90^\circ$, $\chi = 10\%$ and $R/l_1 = 10$, $R = 0.5$ m, $w = 1$ rpm and $\mu = 0.5$.

$110^\circ < \alpha_2 < 140^\circ$, $N_{f \max}$ does not vary so much with α_2 , while it decreases when $\alpha_2 < 110^\circ$ and increases when $\alpha_2 > 140^\circ$. Nevertheless, as explained before, it is not convenient to reduce the value of α_2 below 90° due to the possibility of clogging. A flight is always assumed to be loaded at its maximum capacity at $\delta = 0$, $N_{f \max}$ does not depend on χ . However as illustrated in Fig. 20, it decreases with l_2/l_1 .

Fig. 21 presents the evolution of the number of active flights with α_2 for various l_2/l_1 with $\alpha_1 = 90^\circ$ and $R/l_1 = 10$, $R = 0.5$ m, $w = 1$ rpm and $\mu = 0.5$. It can be observed that since discharging angle range decreases with α_2 , N_{fa} decreases with α_2 . Even if the discharging angle range of the flight increases with l_2/l_1 , the volume carried up by the flights also increases which in turn reduces the maximum number of flights and therefore N_{fa} .

Fig. 22 shows the evolution of the cumulative dimensionless transfer area, of material for all flights and for one drum revolution ζ_{\max}^* , with α_2 . ζ_{\max}^* increases then decreases with α_2 . An optimal value of angle α_2 that permits to maximize ζ_{\max}^* exists for each ratio l_2/l_1 and each value of χ . Globally, we can observe that this optimum angle between flight segments is set in the range $110^\circ - 160^\circ$. As already observed in Fig. 12 and 18, an increase of ratio l_2/l_1 increases the volume of material lifted and released by the flight leading to a higher value of ζ_{\max}^* . An increase of drum filling ratio χ decreases falling height h_f that leads to a decrease of

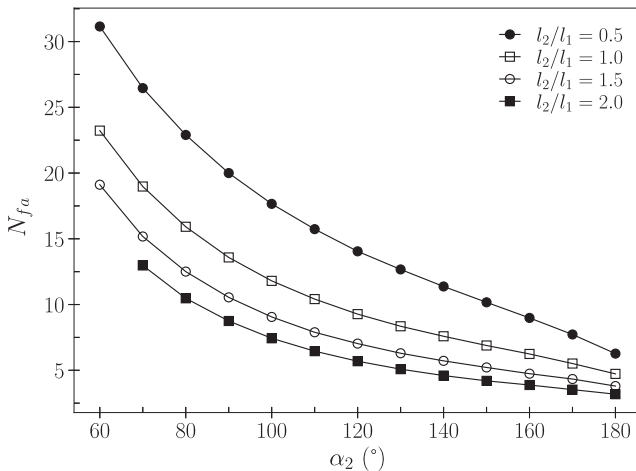


Fig. 21. Number of active flights with α_2 , for various l_2/l_1 with $\alpha_1 = 90^\circ$, $\chi = 10\%$ and $R/l_1 = 10$, $R = 0.5$ m, $w = 1$ rpm and $\mu = 0.5$.

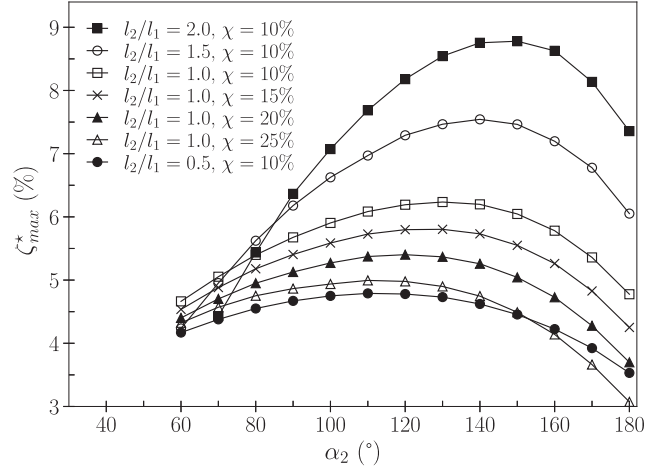


Fig. 22. ζ_{\max}^* with α_2 , for various l_2/l_1 and χ , $\alpha_1 = 90^\circ$, $R/l_1 = 10$, $R = 0.5$ m, $w = 1$ rpm and $\mu = 0.5$.

ζ_{\max}^* as observed in Fig. 22.

4.4. Influence of $\frac{R}{l_1}$

In the design-loaded or over-loaded drum condition, the size ratio when $\alpha_2 = 180^\circ$ must satisfies: $R/l_1 \geq (1 + (l_2/l_1))/(1 - \cos(\beta/2))$. For $l_2/l_1 = 1$, $\alpha_1 = 90^\circ$ and $\chi = 10\%$, we investigated the influence of size ratio R/l_1 in the range $6.5 < R/l_1 < 15$ on ζ_{\max}^* in Fig. 23. It can be observed that ζ_{\max}^* decreases with increasing size ratio R/l_1 . It has been observed that the filling degree of the curtain decreases with R/l_1 while the maximum number of flights that can be set along the drum periphery increases. However, in the range of parameters investigated in this paper, ζ_{\max}^* is more controlled by the flight hold-up than by the falling height or the number of flights. Optimal value lies between $120^\circ < \alpha_2 < 140^\circ$ and tends to decrease with R/l_1 .

Fig. 23 also shows that the variation range of ζ_{\max}^* , over α_2 range, increases when R/l_1 decreases. This illustrates that the choice of α_2 is important to maximize the cumulative transfer area of the material carried by all flights; especially when the drum size ratio R/l_1 is small.

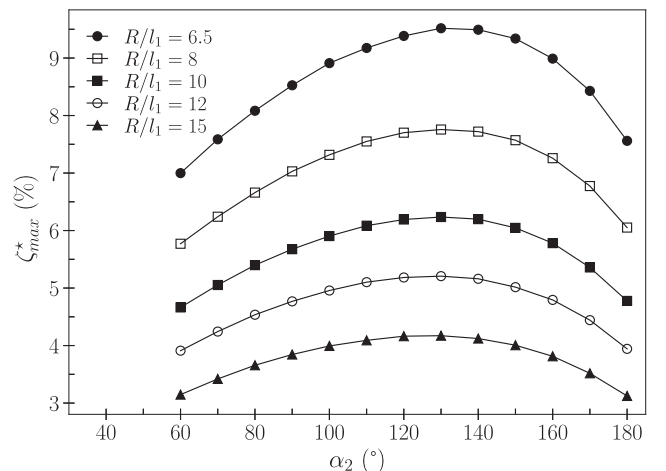


Fig. 23. ζ_{\max}^* with α_2 , for various size ratio R/l_1 for $R = 0.5$ m, $l_2/l_1 = 1$, $\mu = 0.5$, $w = 1$ rpm, $\alpha_1 = 90^\circ$ and $\chi = 10\%$.

5. Conclusion and perspectives

In this paper, a geometrical model has been used to analyse the optimal shape of a two-segmented flight in order to increase the dryer performance of a granular material in a rotating drum. To validate this model, we developed an experimental device that allowed us to measure the volume carried by a flight using image analysis. Our model has been validated by comparison with experimental results obtained in this work and also with results from literature [8,29]. It allowed us to conduct a parametric study. We computed the volume of material carried by the flights and its discharging profile for several values of α_1 , α_2 and l_2/l_1 . Moreover, the influence of drum radius and drum filling ratio have been investigated. Considering the widely used assumption of a vertical fall [8,29,32], assumption that we proved to be reasonable by comparison with our experimental results, we estimated the filling degree of the curtain and the maximum number of flights that can be disposed on the periphery of the drum. Then we computed the cumulative surface of material exposed to the air steam considering contribution of all flights.

The results presented in this paper show that an optimal angle α_2 , between flight segments, exists to maximize the volume of material carried out by each flight. This optimal value tends to increase with ratio l_2/l_1 . For the flight discharge, it has been shown that the uniformity of the discharging profile increases when α_2 decreases. This also leads to an increase in the discharging angle range, which in turn leads to smaller values of the cascading rate. For the falling height of material, it has been observed that, even if it slightly decreases with α_2 , it is mainly affected by the drum filling ratio χ . An increase of χ reduces the falling height.

Curtain filling degree has been integrated over the range of discharging angles leading to the study of the cumulative curtain filling degree ζ_{max} . Results obtained in this work show that the cumulative curtain filling degree increases then decreases with α_2 . The optimum angle α_2 , which maximizes ζ_{max} , is between 110° and 160° . It can also be noted that, on the whole, the cumulative curtain filling degree is higher when the second segment of the flight is longer (higher value of l_2). An increase in the drum filling ratio causes ζ_{max} to decrease. It also tends to lower the optimum angle α_2 for which the cumulative curtain filling degree value is at its maximum. In this study, the influence of the flight connecting angle α_1 on the drum wall has also been investigated. It has been demonstrated that a value of $\alpha_1 = 90^\circ$ is good enough to maximize the cumulative curtain filling degree. Better values can be obtained for α_1 in the range $70^\circ - 80^\circ$, but it seems that these values are not usable for cohesive materials. For such materials, for which flight clogging should be avoided, a slightly larger value of α_1 could sometimes be desired. In such cases, our work shows that the increase of α_1 should be accompanied by a slight decrease of α_2 in order to maintain a high value of cumulative curtain filling ratio.

The maximum number of flights, that can be disposed over the drum periphery to maximize lifted material volume without interfering with other flights is almost constant for $110^\circ < \alpha_2 < 140^\circ$. It decreases with α_2 for $\alpha_2 < 110^\circ$ and increases for $\alpha_2 > 140^\circ$. If we consider that the drum is equipped with this maximum number of flights, we can show that there is an optimal value for the angle between flight segments to maximize the value of the cumulative dimensionless transfer area of material carried by all flights.

To conclude, the results presented in this paper show that with the use of the geometrical model presented and validated in this work, some general recommendations can be stated when considering the optimal flight design. The choice of α_2 is important to maximize the cumulative transfer area of the material carried by all flights especially when the drum size ratio R/l_1 is small. Due to the high number of parameters involved in the flight design, in the drum operational conditions and due to the wide range of material repose angles that can be used in such rotary drum, it is impossible to study all cases. Moreover the use of a quite simple geometrical model is proved to be powerful compared to numerical or experimental studies in terms of time or money cost.

Equations given in this paper can be easily applied to a specific case to help design a specific rotary dryer with specific material.

Declaration of Competing Interest

The authors declare that they have no known competing financial interests or personal relationships that could have appeared to influence the work reported in this paper.

Acknowledgements

The authors gratefully acknowledge financial support from the Centre Mondial de l'Innovation (CMI) Roullier and National Institute of Applied Science (INSA) of Rennes.

Notations

Symbols used

R_0	Distance between the flight extremity and the drum axis
R, D	Drum radius and diameter
l_1, l_2	Length of the flight segments
w	Rotational speed of the drum
g	Acceleration due to gravity
$Fr = w^2 R/g$	Froude number
h_{mat}	Height of material bed
N_{fmax}, N_{fa}	Maximum number of flights and number of active flights respectively
V_{Fi}, A_{Fi}, m_{Fi}	Respectively volume cross-sectional area and mass of material in flight i
f_{Fi}	Ratio between volume of material in flight i and the volume of the drum
c_i	Dimensionless cascading rate
A_{Ci}, m_{Ci}	Local transfer area of curtain i and mass of material released by curtain i
f_{Ci}	Filling degree of the curtain i
d_p	Diameter of particles
h_f, t_f	Falling height and falling time of material
G_{Ci}, G_{Ci}^*	Summation of local transfer area of curtain i over a cascading cycle, starred version is dimensionless one

Greek letters

θ, δ	Angular flight position, angular flight tip position
θ_0, δ_0	Respectively angular flight position and angular flight tip position when flight extremity leaves the material bed
δ_{max}	Angular flight tip position when flight is completely discharged (see Fig. 4)
δ_B	Maximum angular flight tip position for which a falling particle can touch the material bed
θ_0	angular flight position when the flight starts to discharge in the curtain
χ, β	Drum filling ratio, angle defined by surface material bed (see Fig. 1)
γ_f, μ	Material repose angle and dynamic friction coefficient γ_p & dynamic repose angle of material
α_1, α_2	Connecting angle between flight and drum wall, and angle between flight segments (see Fig. 4)
$\eta, \epsilon, \psi, \lambda$	Intermediate angles as defined in Fig. 2 and Fig. 1
ν	Angle between the top of the bed material and an horizontal line passing through the drum section center as described in Fig. 1
ρ_b, ρ_s	Material bulk density, solid density
$\zeta_{max}, \zeta_{max}^*$	Total cumulative transfer area of material carried by all flights during one drum rotation, starred version is dimensionless

References

- [1] D.K. Fidaros, C.A. Baxevanou, C.D. Dritselis, N.S. Vlachos, Numerical modelling of flow and transport processes in a calciner for cement production, *Powder Technol.* 171 (2) (2007) 81–95.
- [2] Y.H. Hui, *Food Drying Science And Technology: Microbiology, Chemistry, Applications*, DEStech Publications, Lancaster, PA, 2008.
- [3] A.S. Mujumdar, *Handbook of Industrial Drying*, CRC Press, Boca Raton, FL, 2014.
- [4] P.G. Glikin, Transport of solids through flighted rotating drums, *Chem. Eng. Res. Des.* 56 (1978) 120–126.
- [5] M. Hellou, F. Lominé, I. Benhsine, Y. Roques, Theoretical description of the motion of a particle in rotary dryer, *Can. J. Chem. Eng.* 97 (2019) 103–114.
- [6] F.R. Schofield, P.G. Glikin, Rotary driers and coolers for granular fertilizers, *Trans. Inst. Chem. Eng.* 40 (1962) 183–190.
- [7] D.R. Van, Puyvelde, Modelling the hold up of lifters in rotary dryers, *Chem. Eng. Res. Des.* 87 (2) (2009) 226–232.
- [8] K.R. Sunkara, F. Herz, E. Specht, J. Mellmann, Influence of flight design on the particle distribution of a flighted rotating drum, *Chem. Eng. Sci.* 90 (2013) 101–109.
- [9] A.Z.M. Abouzeid, D.W. Fuerstenau, A study of the hold-up in rotary drums with discharge end constrictions, *Powder Technol.* 25 (1) (1980) 21–29.
- [10] M.H. Lisboa, D.S. Vitorino, W.B. Delaiba, J.R.D. Finzer, M.A.S. Barrozo, A study of particle motion in rotary dryer, Brazil. *J. Chem. Eng.* 24 (03) (2007) 365–374.
- [11] A.S.B. Njeng, S. Vitu, M. Clausse, J.L. Dirion, M. Debaq, Effect of lifter shape and operating parameters on the flow of materials in a pilot rotary kiln: part I experimental RTD and axial dispersion study, *Powder Technol.* 269 (2014) 554–565.
- [12] M. Kwapinska, G. Saage, E. Tsotsas, Continuous versus discrete modelling of heat transfer to agitated beds, *Powder Technol.* 181 (3) (2008) 331–342.
- [13] F. Geng, Z. Yuan, Y. Yan, D. Luo, H. Wang, B. Li, D. Xu, Numerical simulation on mixing kinetics of slender particles in a rotary dryer, *Powder Technol.* 193 (1) (2009) 50–58.
- [14] I. Benhsine, M. Hellou, F. Lominé, Y. Roques, Influence of flight shape on discharging profiles of granular material in rotary dryer, *EPJ Web Conf.* 140 (2017) 03023.
- [15] D.V. Khakhar, J.J. McCarthy, T. Shinbrot, J.M. Ottino, Transverse flow and mixing of granular materials in a rotating cylinder, *Phys. Fluids* 9 (1) (1998) 31.
- [16] M. Kwapinska, G. Saage, E. Tsotsas, Mixing of particles in rotary drums: A comparison of discrete element simulations with experimental results and penetration models for thermal processes, *Powder Technol.* 161 (1) (2006) 69–78.
- [17] X. Liu, Z. Hu, W. Wu, J. Zhan, F. Herz, E. Specht, DEM study on the surface mixing and whole mixing of granular materials in rotary drums, *Powder Technol.* 315 (2017) 438–444.
- [18] Z. Hu, X. Liu, W. Wu, Study of the critical angles of granular material in rotary drums aimed for fast DEM model calibration, *Powder Technol.* 340 (2018) 563–569.
- [19] B. Chaudhuri, F.J. Muzzio, M.S. Tomassone, Experimentally validated computations of heat transfer in granular materials in rotary calciners, *Powder Technol.* 198 (1) (2010) 6–15.
- [20] L. Leguen, F. Huchet, P. Tamagny, Drying and heating modelling of granular flow: application to the mix-asphalt processes, *J. Appl. Fluid Mech.* 4 (2) (2011) 71–80.
- [21] A.I. Nafsun, F. Herz, E. Specht, V. Scherer, S. Wirtz, Heat transfer experiments in a rotary drum for a variety of granular materials, *Exp. Heat Trans.* 29 (4) (2016) 520–535.
- [22] O.O. Ajayi, M.E. Sheehan, Pseudophysical compartment modeling of an industrial rotary dryer with flighted and unflighted sections: solids transport, *Ind. Ing. Chem. Res.* 53 (2014) 15980.
- [23] M.C.J. Hodgson, W.J. Keast, Rotary dryer flight design, *Proc. Australian Soc. Sugar Cane Technol. Limit.* 6 (1984) 211–218.
- [24] C.G.J. Baker, The design of flights in cascading rotary dryers, *Drying Technol.* 6 (4) (1988) 631–653.
- [25] J. Kelly, Flight design in rotary dryers, *Drying Technol.* 10 (4) (1992) 979–993.
- [26] F.Y. Wang, I.T. Cameron, J.D. Litster, V. Rudolph, A fundamental study on particle transport through rotary dryers for flight design and system optimisation, *Drying Technol.* 13 (5–7) (1995) 1261–1278.
- [27] D. Revol, C.L. Briens, J.M. Chabagno, The design of flights in rotary dryers, *Powder Technol.* 121 (2001) 230–238.
- [28] A. Lee, M.E. Sheehan, Development of a geometric flight unloading model for flighted rotary dryers, *Powder Technol.* 198 (3) (2010) 395–403.
- [29] K.R. Sunkara, F. Herz, E. Specht, J. Mellmann, R. Erpelding, Modeling the discharge characteristics of rectangular flights in a flighted rotary drum, *Powder Technol.* 234 (2013) 107–116.
- [30] A.J. Matchett, C.G. Baker, Particle residence times in cascading rotary dryers part 2 - application of the two-stream model to experimental and industrial data, *J. Separat. Process. Technol.* 9 (1988) 5–13.
- [31] J. Kelly, J.P. O'Donnell, Dynamics of granular material rotary dryers and coolers, *Inst. Chem. Eng. Symp. Ser.* 29 (1968) 33–41.
- [32] W. Blumberg, E.U.U. Schlünder, Transversale schüttgutbewegung und konvektiver stoffübergang in drehrohren teil 2: mit hubschaukeln, *Chem. Eng. Process. Intensific.* 35 (6) (1996) 405–411.
- [33] R.G. Sherritt, R. Caple, L.A. Behie, A.K. Mehrotra, The movement of solids through flighted rotating drums Part i: model formulation, *Can. J. Chem. Eng.* 71 (3) (1993) 337–346.
- [34] F.A. Kamke, J.B. Wilson, Computer simulation of a rotary dryer, Part II Heat Mass Trans. *AIChE J.* 32 (2) (1986) 269–275.
- [35] S.J. Friedman, W.R. Jr. Marshall, Studies in rotary dryer – Part I. Holdup and dusting, *Chem. Eng. Prog.* 45 (8) (1949) 482–493.
- [36] G. Bradski, The OpenCV Library, *Dr. Dobb's J. Soft. Tools* 25 (2000) 120–125.
- [37] C.A. Schneider, W.S. Rasband, K.W. Eliceiri, NIH Image to ImageJ: 25 years of image analysis, *Nat. Methods* 9 (7) (2012) 671–675.